pubs.acs.org/JPCC

Reduction of PEM Fuel Cell Impedance and Resistivity under Simultaneously Applied Oscillations of Potential and Oxygen Supply

Andrei Kulikovsky*



Downloaded via FORSCHUNGZENTRUM JUELICH on December 13, 2024 at 09:06:47 (UTC). See https://pubs.acs.org/sharingguidelines for options on how to legitimately share published articles.

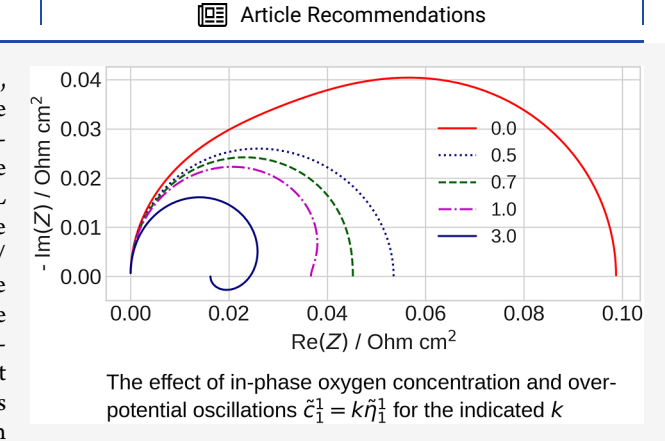
Cite This: J. Phys. Chem. C 2024, 128, 7447-7454



ACCESS I

III Metrics & More

ABSTRACT: Recent model (Electrochem. Comm. 2024, 159, 107655) reveals dramatic decrease of the PEM fuel cell cathode catalyst layer (CCL) impedance under oxygen supply oscillating inphase with the overpotential. Here, a more accurate model for the CCL impedance is developed, and expressions for the static CCL resistivity and polarization curve are derived. The results demonstrate that the resonance pumping of the oxygen concentration at the CCL/ GDL interface with the concentration-to-overpotential amplitude factor k > 0 transfers the CCL to a new steady state with the resistivity and overpotential reduced by a factor $\sim (1 + k)$ in the lowcurrent limit and by (1 + 2k) at high cell currents. To verify the effect in practically relevant conditions, PEM fuel cell impedance is calculated using our 1d + 1d model, assuming that the inlet oxygen



concentration oscillates in-phase with the overpotential. The model includes oxygen transport in the channel and gas-diffusion layer and proton transport in the CCL. The results confirm significant reduction of the cell resistivity, provided that the air flow stoichiometry is large.

INTRODUCTION

The cathode catalyst layer (CCL) in PEM fuel cells has been a subject of numerous studies due to key role of the CCL in the cell performance (see refs 1-3). Basically, any kinetic or transport process in a PEM fuel cell eventually contributes to cell electric resistivity. In particular, the CCL resistivity is a sum of the oxygen reduction reaction (ORR) (faradaic) resistivity and the resistivities of oxygen and proton transport. Lowering CCL resistivity has been among the top priority problems in the fuel cell technology.

One of the best methods for measuring transport and kinetic parameters in an operating CCL is electrochemical impedance spectroscopy (EIS). Typical EIS experiments imply application of small-amplitude harmonic perturbation of current and measurement of the response of cell potential, varying frequency of the applied signal.

Due to intrinsic coupling between the potential, current, and oxygen concentration in PEMFCs, one can generate harmonic oscillations of the cell potential and current by perturbing cathode pressure⁵⁻⁷ or oxygen concentration.⁸⁻¹⁰ The ratio of measured electric to applied nonelectric perturbation amplitudes yields a family of impedance-like spectra. In all the aforementioned methods, a single variable (current, potential, pressure, or oxygen concentration) is perturbed to produce the spectra.

Recently, it has been shown that simultaneously applied inphase oscillations of the ORR overpotential and oxygen concentration at the catalyst/gas diffusion layer (GDL) interface dramatically reduce the CCL impedance and static resistivity.¹¹ Such an EIS-like technique is an interesting option for reduction of the system resistivity rather than the purely diagnostic method.

Below, the effect of resonance pumping of the oxygen concentration in-phase with the ORR overpotential is studied in detail using a more accurate model, which takes into account static oxygen transport loss in the CCL. We show that the CCL resistivity reduces by the factor $\simeq (1 + k)$ at low currents and by (1 + 2k) at high currents, where k is the ratio of applied oscillation amplitudes of the oxygen concentration and overpotential. Finally, the effect is verified using our 1d + 1d model for the PEMFC cathode impedance. In-phase excitation of inlet cathode pressure and overpotential strongly reduces the cell resistivity, provided that the air flow stoichiometry is large.

Received: February 15, 2024 Revised: April 11, 2024 Accepted: April 16, 2024 Published: April 30, 2024





MODEL FOR THE CATALYST LAYER IMPEDANCE

Schematic of the cathode catalyst layer and the boundary conditions for the AC perturbations of the ORR overpotential and oxygen concentration are shown in Figure 1.

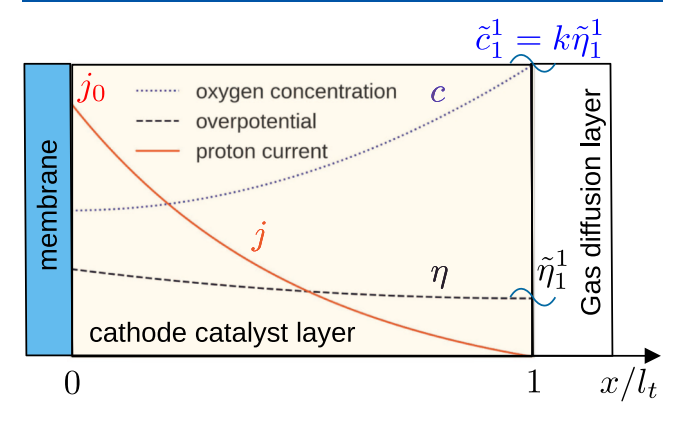


Figure 1. Schematic of the cathode catalyst layer in PEM fuel cell and the typical static shapes of the oxygen concentration, proton current density, and ORR overpotential. Also shown are the boundary conditions for the small AC perturbation amplitudes at the CCL/GDL interface.

The analytical model employs the following assumptions.

- The electron conductivity of the CCL is high.
- Proton transport in the CCL is fast, hence the variation of static and perturbed overpotentials through the CCL depth is negligible.

The assumption of fast proton transport greatly simplifies the analytical treatment of the problem. Numerical calculations below show that the relaxation of this assumption qualitatively does not change the effect predicted by the analytical model.

In ref 11, it was additionally assumed that the oxygen transport in the CCL is fast. Here, this assumption is lifted, allowing us to rationalize the effects at large cell current, when decay of the static oxygen concentration toward the membrane is significant.

The model is based on the proton charge conservation equation

$$C_{\rm dl} \frac{\partial \eta}{\partial t} + \frac{\partial j}{\partial x} = -i_* \left(\frac{c}{c_{\rm ref}} \right) \exp\left(\frac{\eta}{b} \right) \tag{1}$$

and the oxygen mass transport equation

$$\frac{\partial c}{\partial t} - D_{\text{ox}} \frac{\partial^2 c}{\partial x^2} = -\frac{i_*}{4F} \left(\frac{c}{c_{\text{ref}}}\right) \exp\left(\frac{\eta}{b}\right) \tag{2}$$

where x is the distance through the CCL, $C_{\rm dl}$ is the double-layer capacitance, η is the positive by convention ORR overpotential, t is the time, j is the local proton current density, i_* is the ORR volumetric exchange current density, c is the local oxygen concentration, $c_{\rm ref}$ is the reference oxygen concentration, $D_{\rm ox}$ is the CCL oxygen diffusivity, and b is the ORR Tafel slope.

A standard procedure of linearization and Fourier-transform of eqs 1 and 2 leads to the system of linear equations for the small perturbation amplitudes \tilde{j}^1 and \tilde{c}^1 (see mathematical details in and also in section "Resonance nature of k-states")

$$\frac{\partial \tilde{j}^1}{\partial \tilde{x}} = -e^{\tilde{\eta}^0} (\tilde{c}^1 + \tilde{c}^0 \tilde{\eta}^1) - i\tilde{\omega}\tilde{\eta}^1, \quad \tilde{j}^1(1) = 0$$
(3)

$$\begin{split} \tilde{D}_{ox} \frac{\partial^2 \tilde{c}^1}{\partial \tilde{x}^2} &= e^{\tilde{\eta}^0} (\tilde{c}^1 + \tilde{c}^0 \tilde{\eta}^1) + i \mu^2 \tilde{\omega} \tilde{c}^1, \quad \left. \frac{\partial \tilde{c}^1}{\partial \tilde{x}} \right|_{\tilde{x} = 0} = 0, \\ \tilde{c}^1(1) &= k \tilde{\eta}_1^1 \end{split} \tag{4}$$

where

$$\mu \equiv \sqrt{\frac{4Fc_{\rm ref}}{C_{\rm dl}b}} \tag{5}$$

the superscripts 0 and 1 mark the steady-state variables and the small perturbations, respectively. The sign tilde marks dimensionless variables defined according to

$$\tilde{x} = \frac{x}{l_t}, \quad \tilde{t} = \frac{ti_*}{C_{dl}b}, \quad \tilde{c} = \frac{c}{c_{ref}}, \quad \tilde{\eta} = \frac{\eta}{b},$$

$$\tilde{j} = \frac{j}{i_*l_t},$$

$$\tilde{D}_{\text{ox}} = \frac{4FD_{\text{ox}}c_{\text{ref}}}{i_{*}l_{\text{t}}^{2}}, \quad \tilde{Z} = \frac{Zi_{*}l_{t}}{b}, \quad \tilde{\omega} = \frac{\omega C_{\text{dl}}b}{i_{*}},$$
(6)

where ω is the angular frequency of applied AC signal and Z is the CCL impedance. In eqs 3 and 4, $\tilde{\eta}^1$ is the amplitude of overpotential perturbation. Since the charge transport is assumed to be fast, we may set $\tilde{\eta}^1 \simeq \tilde{\eta}^1_1$, where $\tilde{\eta}^1_1$ is the overpotential perturbation applied at the CCL/GDL interface ($\tilde{x}=1$). A key feature of the model is the right boundary condition for eq 4, meaning that the oxygen concentration at the CCL/GDL interface oscillates in-phase with the applied overpotential perturbation $\tilde{\eta}^1_1$, with the amplitude factor k>0.

The equation for the static oxygen concentration is obtained from eq 2 by chalking out the time derivative

$$\tilde{D}_{\text{ox}} \frac{\partial^2 \tilde{c}^0}{\partial \tilde{x}^2} = e^{\tilde{\eta}^0} \tilde{c}^0, \quad \tilde{c}^0(1) = \tilde{c}_1^0$$
(7)

Solution to eq 7 is

$$\tilde{c}^{0}(\tilde{x}) = \frac{\tilde{c}_{1}^{0} \cosh(\phi \tilde{x})}{\cosh \phi}, \quad \phi \equiv \sqrt{\frac{e^{\tilde{\eta}^{0}}}{\tilde{D}_{ox}}}$$
(8)

Introducing local concentration G and electric Y admittances

$$G \equiv \frac{\tilde{c}^1}{\tilde{\eta}^1}, \quad Y \equiv \frac{\tilde{j}^1}{\tilde{\eta}^1} \tag{9}$$

and noting that $\tilde{\eta}^1$ is nearly constant along \tilde{x} , we can divide eqs 3 and 4 by $\tilde{\eta}^1$, which leads to the problem for $Y(\tilde{x})$ and $G(\tilde{x})$

$$\frac{\partial Y}{\partial \tilde{x}} = -e^{\tilde{\eta}^0} (G + \tilde{c}^0) - i\tilde{\omega}, \quad Y(1) = 0$$
(10)

$$\tilde{D}_{ox} \frac{\partial^2 G}{\partial \tilde{x}^2} = e^{\tilde{\eta}^0} (G + \tilde{c}^0) + i\mu^2 \tilde{\omega} G, \qquad \frac{\partial G}{\partial \tilde{x}} \bigg|_{\tilde{x}=0} = 0,$$

$$G(1) = k \tag{11}$$

Solution to eq 11 with $\tilde{c}^0(\tilde{x})$, eq 8, is

$$G(\tilde{x}) = \frac{(\tilde{c}_{1}^{0} e^{\tilde{\eta}^{0}} + ki\tilde{\omega}\mu^{2})\cosh(\tilde{x}/\sqrt{\tilde{Z}_{ct}\tilde{D}_{ox}})}{i\tilde{\omega}\mu^{2}\cosh(1/\sqrt{\tilde{Z}_{ct}\tilde{D}_{ox}})}$$
$$-\frac{\tilde{c}_{1}^{0} e^{\tilde{\eta}^{0}}\cosh(\phi\tilde{x})}{i\tilde{\omega}\mu^{2}\cosh(\phi)}$$
(12)

where

$$\tilde{Z}_{ct} \equiv \frac{1}{e^{\tilde{\eta}^0} + i\tilde{\omega}\mu^2} \tag{13}$$

is the charge-transfer (parallel *RC*-circuit) impedance. Finally, solution of eq 10 with eq 12 for $G(\tilde{x})$ gives the CCL impedance $\tilde{Z} = 1/Y|_{\tilde{x}=0}$

$$\tilde{Z} = i\tilde{\omega}\mu^{2} \left(\tilde{c}_{1}^{0} e^{\tilde{\eta}^{0}} (i\tilde{\omega}\mu^{2} - e^{\tilde{\eta}^{0}}) \frac{\tanh(\phi)}{\phi} - \tilde{\omega}^{2}\mu^{2} \right)$$

$$+ e^{\tilde{\eta}^{0}} (ki\tilde{\omega}\mu^{2} + \tilde{c}_{1}^{0} e^{\tilde{\eta}^{0}}) \tilde{Z}_{W} \right)^{-1}$$

$$(14)$$

where ϕ is given in eq 8 and

$$\tilde{Z}_{\rm W} \equiv \frac{\tanh(1/\sqrt{\tilde{Z}_{\rm ct}\tilde{D}_{\rm ox}})}{1/\sqrt{\tilde{Z}_{\rm ct}\tilde{D}_{\rm ox}}} \tag{15}$$

is the Warburg-like finite length impedance.

RESULTS AND DISCUSSION

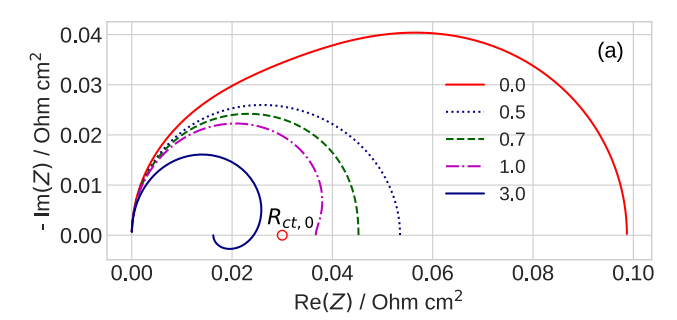
To illustrate the results, below the Tafel equation for the static polarization curve is used to relate the static cell current density j_0 and overpotential η^0 . With the dimensionless variables eq 6, this equation has the form

$$\tilde{j}_0 = \tilde{c}_1^0 \exp \tilde{\eta}^0 \tag{16}$$

Strictly speaking, eq 16 does not hold at high cell currents due to "transport" Tafel slope doubling (see below), neither it describes kinetic growth of the Tafel slope with the cell current density. ¹³ In general, the analysis below could be done in terms of the static cell potential, keeping the factor \tilde{c}_1^0 exp $\tilde{\eta}^0$ in eq 14. However, eq 16 helps clarify and illustrate qualitatively the key effects due to oxygen concentration oscillations.

CCL Impedance Spectra. Figure 2a shows the Nyquist spectra of the CCL impedance, eq 14, for the set of $k = \{0, 0.5, 0.7, 1, 3\}$ and the cell current density of 1 A cm⁻². The other parameters for the calculations are gathered in Table 1. Qualitatively, the effect of k on the cell impedance in Figure 2a is similar to the effect at low cell current: 11 the impedance modulus and the static CCL resistivity decrease with the increase in k. Figure 2b shows that with the growth of k, the oxygen diffusion peak vanishes, while the right faradaic "shoulder" transforms into a distinct peak, which decreases in the amplitude.

Figure 3a shows the phase angle $\arg(G)$ along \tilde{x} calculated using eq 12. With k=0, the phase angle between \tilde{c}^1 and $\tilde{\eta}^1$ is large through the whole CCL depth, excluding a singe point $\tilde{x}=1$ (Figure 3a). However, already at k=0.5, nearly half of the CCL thickness operates at $\arg(G)\simeq 0$, meaning that in this domain, the oxygen concentration oscillates in-phase with the overpotential. Further growth of k extends the region of reduced l $\arg(G)l$ down to the membrane (Figure 3a). Smallness of the phase shift between \tilde{c}^1 and $\tilde{\eta}^1$ means strongly reduced oxygen



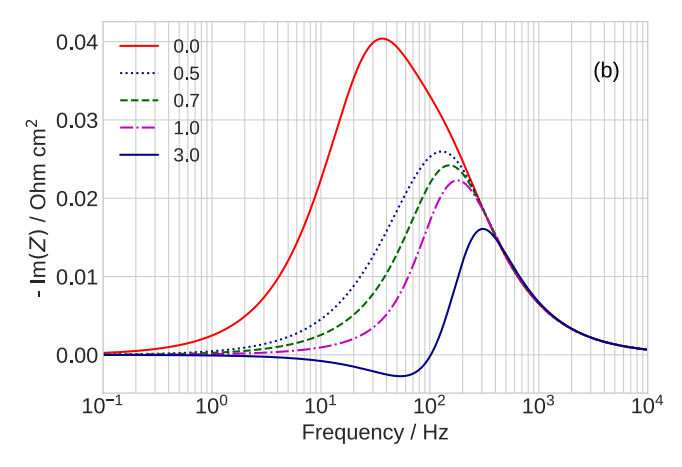


Figure 2. (a) Nyquist spectra of the CCL, eq 14, for the indicated values of parameter k in eq 4 and the cell current density of 1 A cm⁻². The other parameters are listed in Table 1. The point $R_{\rm ct,0}$ indicates the estimate of static charge-transfer resistivity b/j_0 at k=0. (b) The frequency dependence of the imaginary part of impedances in (a).

Table 1. Cell Parameters Used in Calculations^a

Tafel slope b, V	0.03
double-layer capacitance $C_{\rm dl}$, F cm ⁻³	20
exchange current density i*, A cm ⁻³	10^{-3}
oxygen diffusion coefficient in the CCL, D_{ox} , cm ² s ⁻¹	1×10^{-4}
catalyst layer thickness l_v cm	12×10^{-4}
cell temperature T, K	273 + 80
cathode pressure, bar	1.5
cathode relative humidity, %	50
cell current density j_0 , A cm ⁻²	1.0

^aParameter D_{ox} is taken to be small to emphasize the effect of oxygen transport in the CCL.

transport losses in this domain, which leads to significant growth of the transient ORR rate (Figure 3b). Both effects dramatically lower the CCL impedance and eventually the static CCL resistivity.

Finite proton conductivity qualitatively does not change the results. Substituting the Ohm's law $\tilde{j}^1=-\varepsilon^2\partial\tilde{\eta}^1/\partial\tilde{x}$ into eq 3 we get

$$\varepsilon^{2} \frac{\partial^{2} \tilde{\eta}^{1}}{\partial \tilde{x}^{2}} = e^{\tilde{\eta}^{0}} (\tilde{c}^{1} + \tilde{c}^{0} \tilde{\eta}^{1}) + i \tilde{\omega} \tilde{\eta}^{1}, \quad \frac{\partial \tilde{\eta}^{1}}{\partial \tilde{x}} \bigg|_{\tilde{x}=1} = 0,$$

$$\tilde{\eta}^{1}(1) = \tilde{\eta}_{1}^{1} \tag{17}$$

where ε is the dimensionless Newman's reaction penetration depth

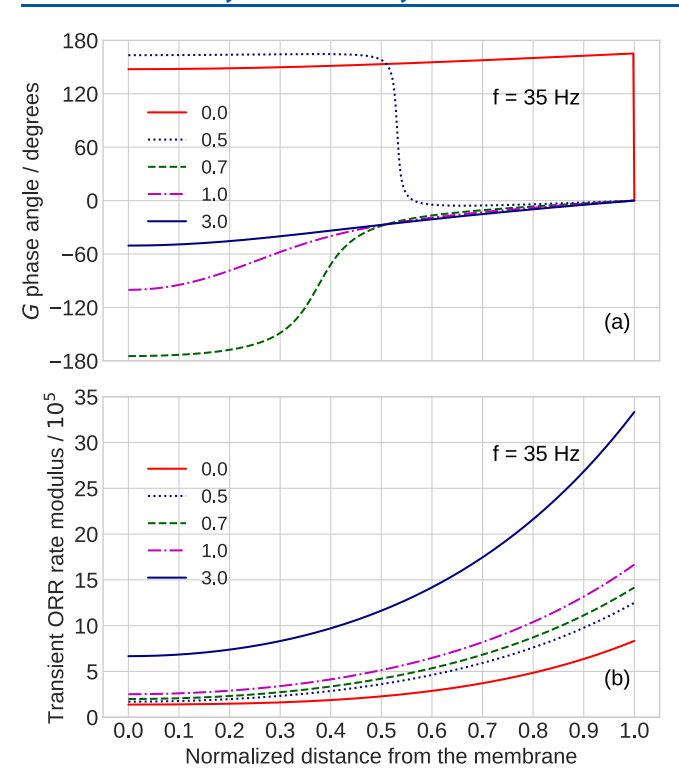


Figure 3. (a) Phase angle of $G = \tilde{c}^1/\tilde{\eta}_1^1$ (between oxygen concentration and overpotential) vs distance \tilde{x} through the CCL. The frequency of 35 Hz corresponds to the position of the transport peak in Figure 2b (red curve). (b) Dimensionless modulus of the transient ORR rate (the right side of eq 4, $e^{\tilde{\eta}^0}(\tilde{c}^1 + \tilde{c}^0\tilde{\eta}^1) + i\mu^2\tilde{\omega}\tilde{c}^1$) calculated at the frequency of 35 Hz.

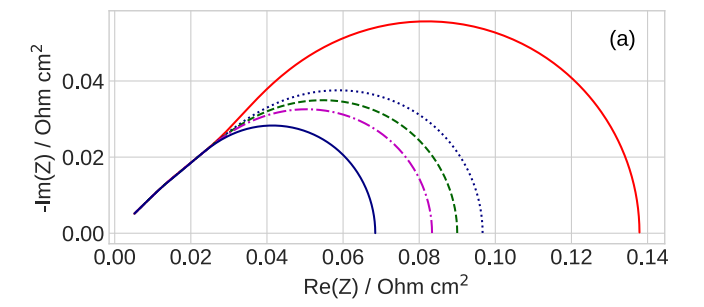
$$\varepsilon = \sqrt{\frac{\sigma_{\rm p} b}{i_* l_{\rm t}^2}} \tag{18}$$

and σ_p is the CCL proton conductivity. Numerical solutions of systems (4) and (17) give the spectra shown in Figure 4. The CCL proton conductivity used in the calculations is 15 mS cm⁻¹; the other parameters are listed in Table 1. Comparing Figures 2 and 4, we see that finite proton conductivity increases the CCL impedance; however, the qualitative trend of impedance reduction upon increase in k in both figures is the same. For example, with k=3, the total CCL polarization resistivity in Figure 4a is reduced by a factor of 2.

CCL Static Resistivity and Polarization Curve. From eq 14, equations for the static CCL resistivity and polarization curve can be derived. For brevity, the CCL "post-oscillating" steady state at $\tilde{\omega} \rightarrow 0$ and k > 0 will be referred to as the k-state. To understand the numerical results, it is advisable to calculate the CCL static resistivity $\tilde{R}_k = \lim_{\tilde{\omega} \rightarrow 0} \tilde{Z}$ in the k-state. From eq 14, we find

$$\tilde{R}_k = \frac{2}{\tilde{D}_{ox}\phi((\tilde{c}_1^0 + 2k)\tanh(\phi) + \tilde{c}_1^0\phi/\cosh(\phi)^2)}$$
(19)

where $\phi = \sqrt{{\rm e}^{\tilde{\eta}^0}/\tilde{D}_{\rm ox}}$. Consider first the case of the small cell current density. Since $\phi \sim \sqrt{j_0}$, we can expand eq 19 in Taylor series at $\phi = 0$. Keeping two leading terms, we get



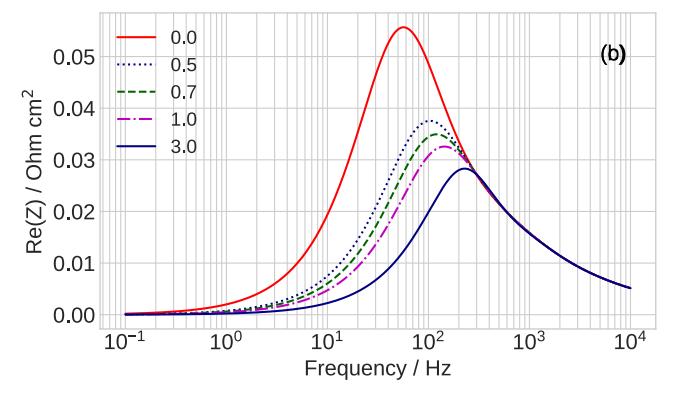


Figure 4. (a) Nyquist spectra of the CCL with the finite rate of proton transport. Indicated are the values of parameter k; the cell current density is 1 A cm⁻², and the CCL proton conductivity is 15 mS cm⁻¹. The other parameters are listed in Table 1. (b) Frequency dependence of the imaginary part of impedances in (a).

$$\tilde{R}_k \simeq \frac{1}{(1+k)\tilde{j}_0} + \frac{2+k}{3(1+k)^2 \tilde{D}_{ox}}, \quad \frac{\tilde{j}_0}{\tilde{D}_{ox}} \ll 1$$
 (20)

Here, the problem of CCL impedance only is considered, and c_1^0 is the static oxygen concentration at the CCL/GDL interface. Without loss of generality, this concentration can be set equal to the reference oxygen concentration, leading to $\tilde{c}_1^{\ 0}=1$. Keeping the concentration factor in eqs. 19–25 would make the formulas more cumbersome only but it would not change the physics and/or scaling. The inequality $\tilde{j}_0/\tilde{D}_{\rm ox}\ll 1$ in the dimension form reads $j_0/(4FD_{\rm ox}c_{\rm ref}/l_{\rm t})\ll 1$, meaning that the cell current density must be much less than the characteristic current density $4FD_{\rm ox}c_{\rm ref}/l_{\rm t}$ of oxygen transport in the CCL.

Evidently, the first term in eq 20 is the faradaic (charge-transfer) resistivity $R_{\rm ct}$, and the second term gives the resistivity due to finite rate of oxygen diffusion. As can be seen, oxygen pumping lowers $R_{\rm ct}$ by the factor of (1 + k). Note that nonuniformity of the static oxygen concentration doubles the oxygen transport resistivity. Indeed, at k = 0, the second term in eq 20 in the dimension form is

$$R_{\rm ox} = \frac{2bl_t}{3(4FD_{\rm ox}c_{\rm ref})} \tag{21}$$

which is twice larger than the oxygen transport resistivity $R_{\rm ox}$ under negligible static oxygen transport loss in the CCL. ¹⁴ Thus, it makes sense to write eq 20 in the form

$$\tilde{R}_k \simeq \frac{1}{(1+k)\tilde{j}_0} + \frac{1}{3(1+k)\tilde{D}_{ox}} + \frac{1}{3(1+k)^2\tilde{D}_{ox}}$$
 (22)

where the second term on the right side is the oxygen transport resistivity at weakly nonuniform static oxygen concentration $\tilde{c}^0(\tilde{x})$ through the CCL and the last term is the transport resistivity due to $\tilde{c}^0(\tilde{x})$ non-uniformity. In the dimension form, eq 22 is

$$R_{k} \simeq \frac{b}{(1+k)j_{0}} + \frac{bl_{t}}{3(1+k)4FD_{\text{ox}}c_{\text{ref}}} + \frac{bl_{t}}{3(1+k)^{2}4FD_{\text{ox}}c_{\text{ref}}}$$
(23)

The static polarization curve of the CCL in the k-state is obtained from equation

$$\frac{\partial \tilde{\eta}_k^0}{\partial \tilde{j}_0} = \tilde{R}_k \tag{24}$$

Integrating eq 24 with \tilde{R}_k , eq 22, and omitting insignificant integration constant, we come to the low-current curve

$$\tilde{\eta}_k^0 \sim \frac{\ln(\tilde{j}_0)}{1+k} + \frac{\tilde{j}_0}{3(1+k)\tilde{D}_{ox}} + \frac{\tilde{j}_0}{3(1+k)^2\tilde{D}_{ox}}$$
 (25)

Obviously, the first term is the Tafel activation overpotential, and the sum of the second and third terms is the oxygen transport overpotential.

Importantly, all the terms in eqs 22 and 25 decrease with the growth of k. This means that the resonance pumping of oxygen concentration at the CCL/GDL interface with the amplitude factor k, in the limit of zero $\tilde{\omega}$ transfers the system to a new steady-state with $\gtrsim (1+k)$ times lower static resistivity. More specifically, eq 25 shows that in the k-state, the ORR activation overpotential is reduced by the factor (1+k), and the transport overpotential is reduced by the factor $\gtrsim (1+k)$.

In the opposite limit of large current density, the leading term of asymptotic expansion of eq 19 over large ϕ is

$$\tilde{R}_k \simeq \frac{2}{(1+2k)\sqrt{\tilde{j}_0\tilde{D}_{ox}}}, \quad \frac{\tilde{j}_0}{\tilde{D}_{ox}} \gg 1$$
(26)

In the dimension form, eq 26 reads

$$R_k \simeq \frac{2b}{(1+2k)} \sqrt{\frac{l_t}{4FD_{\rm ox}c_{\rm re}j_0}}$$
 (27)

Integrating eq 24 with \tilde{R} , eq 26, we find

$$\tilde{\eta}_k^0 \sim \frac{4}{1+2k} \sqrt{\frac{\tilde{j}_0}{\tilde{D}_{\text{ox}}}}$$
 (28)

At large cell currents, the transport and reaction activation overpotentials are merged into one term. The Tafel exponential dependence of current on the overpotential vanishes, and we get a much slower quadratic dependence instead. However, as in the low-current limit, with the growth of k, the resistivity and overpotential decrease. Note that the k-state at high currents is even more beneficial as the reduction factor (1 + 2k) in eq 26 grows with k faster than the low-current factor (1 + k) in eq 22.

Figure 5a demonstrates lowering of the CCL resistivity R_k in the k-state, eq 19, in the range of cell current densities from 10 mA cm $^{-2}$ to 2 A cm $^{-2}$ for the set of parameters k. As can be seen, with k=3, the effect at $j_0=1$ A cm $^{-2}$ is dramatic: the lowering of R_k is about an order of magnitude. Figure 5b shows the static polarization curves of the CCL for the same values of parameter k. Here, the overpotential η_k is calculated by numerical

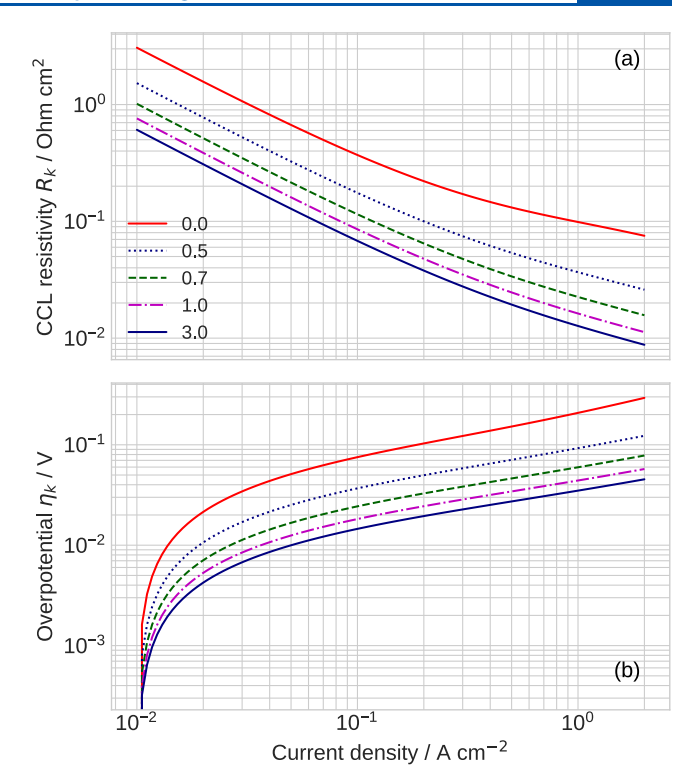


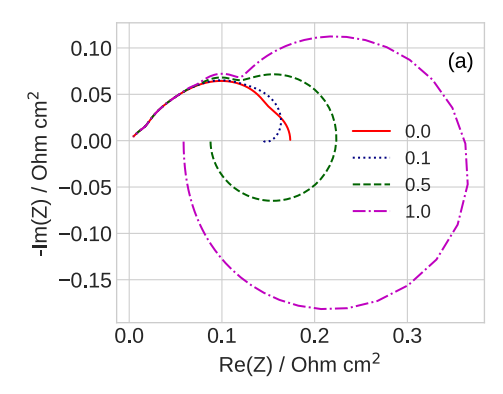
Figure 5. (a) Dependence of CCL static resistivity R, eq 19, on the cell current density j_0 for the indicated values of parameter k. (b) Static CCL polarization curves for the same value of k.

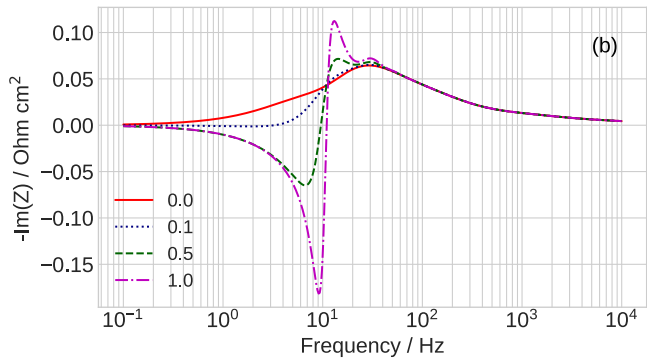
integration of \tilde{R}_k , eq 19, over \tilde{j}_0 . At 1 A cm⁻² and k = 3, the CCL overpotential decreases from 200 to 35 mV (Figure 5b).

Spectra from the 1d + 1d Cell Impedance Model. In practice, direct application of the oxygen concentration oscillations at the CCL/GDL interface is hardly feasible. However, the oxygen concentration can be perturbed in the cathode channel by applying pressure and/or flow velocity oscillations at the channel inlet. Figure 6 shows the spectra calculated using the full 1d + 1d impedance model, 15,16 which takes into account oxygen transport in the air channel and GDL and proton transport in the CCL. The air flow stoichiometry is λ = 10, the GDL oxygen diffusivity is taken to be $0.02 \text{ cm}^2 \text{ s}^{-1}$, and the cell current density is 0.4 A cm⁻²; the other cell parameters are listed in Table 1. The oxygen concentration $\tilde{c}_h^1(z=0)$ at the channel inlet (z) is the coordinate along the channel is perturbed according to $\tilde{c}_h^1(0) = k\tilde{\eta}_1^1$, where $\tilde{\eta}_1^1$ is the applied overpotential perturbation. In other words, the inlet pressure and oxygen concentration oscillate in phase with the overpotential. The flow velocity oscillations induced by the inlet pressure perturbation are calculated as described in.1

Calculations show that at high air flow stoichiometry, the applied oscillations of the inlet oxygen concentration propagate down the channel with no or minor variation in the phase. Moreover, at low frequencies, the GDL does not change the phase of the transported oxygen concentration oscillations. Both effects allow the low-frequency oscillations of inlet oxygen concentration to penetrate the CCL/GDL interface with no phase change. This provides significant reduction of the cell impedance at frequencies below 5 Hz and of the static cell resistivity (Figure 6).

Kim et al. ¹⁸ and Hwang et al. ¹⁹ applied harmonic oscillations of the cathode flow velocity and measured significant improve-





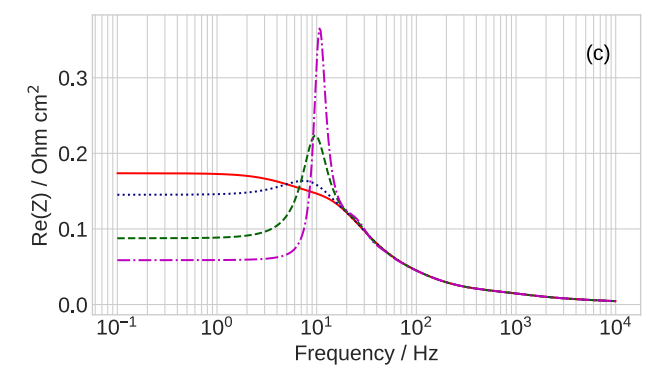


Figure 6. (a) Nyquist spectra calculated for the indicated parameters k using the full 1d + 1d impedance model. The air flow stoichiometry is 10, the GDL oxygen diffusivity is 0.02 cm² s⁻¹, and the cell current density is 0.4 A cm⁻²; the other parameters are listed in Table 1. (b,c) Frequency dependence of imaginary and real part of impedances in (a).

ment of the PEMFC performance. Figure 7 shows the experimental polarization curves¹⁸ at zero $(V_{pp} = 0)$ and non-

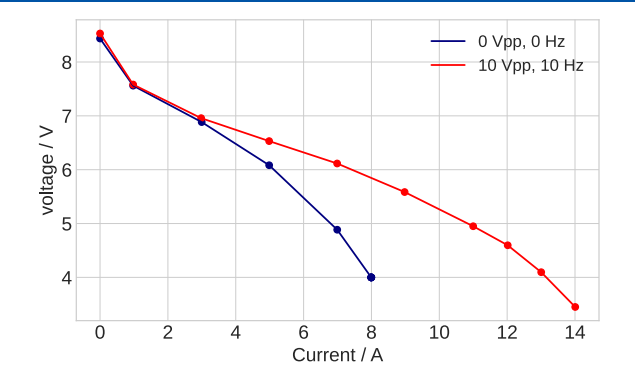


Figure 7. Cell polarization curves measured at zero (0 $V_{\rm pp}$, 0 Hz) and non-zero (10 $V_{\rm pp}$, 10 Hz) flow velocity oscillation amplitude in experiments of Kim et al. ¹⁸.

zero $(10V_{\rm pp})$ amplitudes of the inlet flow velocity oscillations. The flow velocity oscillations were produced applying 10 Hz pressure oscillations by means of acoustic woofer; $V_{\rm pp}$ is the potential applied to the woofer. As can be seen, flow pressure/velocity oscillations dramatically improve the cell performance.

Kim et al. explained the effect by improved oxygen diffusive transport in porous layers, although no mechanism of this improvement has been discussed. In their experiments, no external potential perturbation has been applied to the cell; however, flow pressure/velocity oscillations inevitably generate this perturbation, and the improvement of cell performance could be due to the mechanism described above. Further experiments of this type are highly desirable.

Resonance Nature of *k***-States.** Equations 3 and 4 are obtained from the dimensionless versions of eqs 1 and 2 by substitution of Fourier transforms

$$\tilde{y}(\tilde{x}, \tilde{t}) = \tilde{y}^{0}(\tilde{x}) + \tilde{y}^{1}(\tilde{x}, \tilde{\omega}) \exp(i\tilde{\omega}\tilde{t}), \quad |\tilde{y}^{1}| \ll \tilde{y}^{0}$$
 (29)

into eqs 1 and 2, where \tilde{y} stands for $\tilde{\eta}$, \tilde{c} , and \tilde{j} . Expanding exponents in eqs 1 and 2 in Taylor series, keeping two leading terms, subtracting the static equations, and neglecting the terms with perturbation products, we get eqs 3 and 4.

Consider eq 29 written for \tilde{c}

$$\tilde{c}(\tilde{x}) = \tilde{c}^{0}(\tilde{x}) + \tilde{c}^{1}(\tilde{x}, \,\tilde{\omega}) \exp(i\tilde{\omega}\tilde{t})$$
(30)

At $\tilde{x} = 1$ we get

$$\tilde{c}(1) = \tilde{c}_1^0 + k\tilde{\eta}_1^1 \exp(i\tilde{\omega}\tilde{t})$$
(31)

In the limit of $\tilde{\omega} = 0$, from eq 31 we find

$$\tilde{c}_1 = \tilde{c}_1^0 + k\tilde{\eta}_1^1 \tag{32}$$

where the subscript 1 marks the values at $\tilde{x}=1$. Thus, the "post-oscillatory" steady state corresponding to k>0 (the k-state) differs from the steady state corresponding to k=0 by a small constant additive $k\tilde{\eta}_1^1$ to the oxygen concentration \tilde{c}_1^0 at the CCL/GDL interface. Surprisingly, this small additive dramatically decreases the static cell resistivity.

It is important, however, that in eq 31, the additive amplitude $k\tilde{\eta}_1^1$ is proportional to the overpotential amplitude. At finite $\tilde{\omega}$, this proportionality provides resonance character of impedance lowering: upon increase in ORR overpotential, the oxygen concentration also increases, reducing the system impedance. In the limit of $\tilde{\omega} \rightarrow 0$, this resonance transfers the system to the steady state with strongly reduced resistivity. It follows that the static k-states could be reached only from the transient k-states by lowering the AC signal frequency.

CONCLUSIONS

A recent model for the cathode catalyst layer impedance under simultaneously applied oscillations of overpotential and oxygen concentration is extended to take into account nonuniformity of the static oxygen concentration through the CCL depth. Analytical solution for the CCL impedance at the cell current density of 1 A cm $^{-2}$ under simultaneously applied in-phase oscillations of the oxygen concentration and overpotential is derived. Equations for the static cell resistivity and polarization curve are obtained. As in the low-current case, an increase in the amplitude of applied perturbations of the oxygen concentration leads to dramatic reduction of the CCL low-frequency impedance and static resistivity R_k . At low currents, the faradaic resistivity is reduced by a factor of (1+k), and the oxygen

transport resistivity is decreased by a factor of $\gtrsim (1+k)$, where k is the ratio of the applied oxygen concentration to overpotential amplitudes. At large currents, the faradaic and transport resistivities are merged in one term, which is reduced by a factor of (1+2k). The effect of PEM fuel cell static resistivity reduction is confirmed numerically for realistic operating conditions by means of the 1d+1d impedance model, assuming that the inlet cathode pressure and oxygen concentration oscillate in-phase with the applied AC perturbations of the overpotential. If the air flow stoichiometry is large, low-frequency inlet oxygen perturbation penetrates to the CCL/GDL interface with no or minimal phase change, providing reduction of the cell impedance and static resistivity.

AUTHOR INFORMATION

Corresponding Author

Andrei Kulikovsky — Forschungszentrum Jülich GmbH, Theory and Computation of Energy Materials (IEK-13), Institute of Energy and Climate Research, D-52425 Jülich, Germany; orcid.org/0000-0003-1319-576X; Email: a.kulikovsky@fz-juelich.de

Complete contact information is available at: https://pubs.acs.org/10.1021/acs.jpcc.4c01010

Notes

The author declares no competing financial interest.

ACKNOWLEDGMENTS

The authors thank Forschungszentrum Jülich for support during this work.

■ NOMENCLATURE

- ~ marks dimensionless variables
- b ORR Tafel slope, V
- $C_{\rm dl}$ double-layer volumetric capacitance, F cm⁻³
- c oxygen molar concentration in the CCL, mol cm^{-3}
- c_h oxygen molar concentration in the channel, mol cm⁻³
- $c_{\rm ref}$ reference oxygen concentration, mol cm⁻³
- $D_{\rm ox}$ oxygen diffusion coefficient in the CCL, cm² s⁻¹
- F Faraday constant, C mol⁻¹
- f frequency, Hz
- G dimensionless concentration admittance $\tilde{c}^1/\tilde{\eta}_1^1$
- j local proton current density, A cm⁻²
- j_0 cell current density, A cm⁻²
- *i* imaginary unit
- i* ORR volumetric exchange current density, A cm⁻³
- k concentration amplitude factor, eq
- $l_{\rm t}$ catalyst layer thickness, cm
- R static resistivity, Ω cm²
- $R_{\rm ct}$ static charge-transfer resistivity, Ω cm²
- t time, s
- x coordinate through the cell, cm
- Y dimensionless electric admittance $\tilde{i}^1/\tilde{\eta}^1$
- z coordinate along the cathode channel, cm
- Z CCL impedance, Ω cm²
- $Z_{\rm ct}$ charge-transfer impedance, eq ¹³, Ω cm²
- $Z_{\rm W}$ Warburg finite length impedance, eq ¹⁵, Ω cm²

SUBSCRIPTS:

- 0 membrane/CCL interface
- 1 CCL/GDL interface

SUPERSCRIPTS:

- 0 steady-state value
- 1 small perturbation amplitude

GREEK:

- arepsilon dimensionless Newman's reaction penetration depth, eq 18
- η ORR overpotential, positive by convention, V
- η_1^1 amplitude of applied overpotential perturbation, V
- μ dimensionless parameter, eq
- ϕ dimensionless parameter, eq
- ω angular frequency of the AC signal, s⁻¹

REFERENCES

- (1) Huang, J.; Li, Z.; Zhang, J. Review of Characterization and Modeling of Polymer Electrolyte Fuel Cell Catalyst Layer: The Blessing and Curse of Ionomer. *Front. Energy* **2017**, *11*, 334–364.
- (2) Deng, X.; Zhang, J.; Fan, Z.; Tan, W.; Yang, G.; Wang, W.; Zhou, W.; Shao, Z. Understanding and Engineering of Multiphase Transport Processes in Membrane Electrode Assembly of Proton-Exchange Membrane Fuel Cells with a Focus on the Cathode Catalyst Layer: A Review. *Energy Fuels* **2020**, *34*, 9175–9188.
- (3) Olbrich, W.; Kadyk, T.; Sauter, U.; Eikerling, M. Review-Wetting Phenomena in Catalyst Layers of PEM Fuel Cells: Novel Approaches for Modeling and Materials Research. *J. Electrochem. Soc.* **2022**, *169*, 054521.
- (4) Lasia, A. Electrochemical Impedance Spectroscopy and its Applications; Springer: New York, 2014.
- (\$) Engebretsen, E.; Mason, T. J.; Shearing, P. R.; Hinds, G.; Brett, D. J. L. Electrochemical Pressure Impedance Spectroscopy Applied to the Study of Polymer Electrolyte Fuel Cells. *Electrochem. Commun.* **2017**, 75, 60–63.
- (6) Shirsath, A. V.; Rael, S.; Bonnet, C.; Schiffer, L.; Bessler, W.; Lapicque, F. Electrochemical Pressure Impedance Spectroscopy for Investigation of Mass Transfer in Polymer Electrolyte Membrane Fuel Cells. *Curr. Opin. Electrochem.* **2020**, *20*, 82–87.
- (7) Zhang, Q.; Homayouni, H.; Gates, B. D.; Eikerling, M.; Niroumand, A. M. Electrochemical Pressure Impedance Spectroscopy for Polymer Electrolyte Fuel Cells via Back-Pressure Control. *J. Electrochem. Soc.* **2022**, *169*, 044510.
- (8) Sorrentino, A.; Vidakovic-Koch, T.; Hanke-Rauschenbach, R.; Sundmacher, K. Concentration—Alternating Frequency Response: A New Method for Studying Polymer Electrolyte Membrane Fuel Cell Dynamics. *Electrochim. Acta* **2017**, 243, 53–64.
- (9) Sorrentino, A.; Vidakovic-Koch, T.; Sundmacher, K. Studying Mass Transport Dynamics in Polymer Electrolyte Membrane Fuel Cells using Concentration—Alternating Frequency Response Analysis. *J. Power Sources* **2019**, *412*, 331–335.
- (10) Sorrentino, A.; Sundmacher, K.; Vidakovic-Koch, T. Polymer Electrolyte Fuel Cell Degradation Mechanisms and Their Diagnosis by Frequency Response Analysis Methods: A Review. *Energies* **2020**, *13*, 5825
- (11) Kulikovsky, A. Performance of a PEM Fuel Cell Cathode Catalyst Layer under Oscillating Potential and Oxygen Supply. *Electrochem. Commun.* **2024**, *159*, 107655.
- (12) Kulikovsky, A. A. Analytical Physics—Based Impedance of the Cathode Catalyst Layer in a PEM Fuel Cell at Typical Working Currents. *Electrochim. Acta* **2017**, 225, 559—565.
- (13) Jackson, C.; Lin, X.; Levecque, P. B. J.; Kucernak, A. R. J. Toward Understanding the Utilization of Oxygen Reduction Electrocatalysts under High Mass Transport Conditions and High Overpotentials. *ACS Catal.* **2022**, *12*, 200–211.
- (14) Kulikovsky, A. A. One–Dimensional Impedance of the Cathode Side of a PEM Fuel Cell: Exact Analytical Solution. *J. Electrochem. Soc.* **2015**, *162*, F217–F222.
- (15) Reshetenko, T.; Kulikovsky, A. A Model for Extraction of Spatially Resolved Data from Impedance Spectrum of a PEM Fuel Cell. *J. Electrochem. Soc.* **2018**, *165*, F291–F296.

- (16) Kulikovsky, A. Analytical Models for PEM Fuel Cell Impedance; Self-publishing: Eisma, 2022.
- (17) Kulikovsky, A. Flow Velocity Oscillations in a PEM Fuel Cell Cathode Channel Induced by Harmonic Pressure Perturbations. *J. Power Sources* **2023**, *558*, 232544.
- (18) Kim, Y. H.; Han, H. S.; Kim, S. Y.; Rhee, G. H. Influence of Cathode Flow Pulsation on Performance of Proton—Exchange Membrane Fuel Cell. *J. Power Sources* **2008**, *185*, 112—117.
- (19) Hwang, Y.-S.; Lee, D.-Y.; Choi, J. W.; Kim, S.-Y.; Cho, S. H.; Joonho, P.; Kim, M. S.; Jang, J. H.; Kim, S. H.; Cha, S.-W. Enhanced Diffusion in Polymer Electrolyte Membrane Fuel Cells Using Oscillating Flow. *Int. J. Hydrogen Energy* **2010**, *35*, 3676–3683.